03

High-resolution visualization of the gravitational separation of a water drop under an electrostatic field

© Yu.D. Chashechkin, V.E. Prokhorov

Ishlinsky Institute for Problems in Mechanics, Russian Academy of Sciences,
119526 Moscow, Russia
e-mail: yulidch@gmail.com

Received June 19, 2023
Revised September 19, 2023
Accepted September 21, 2023

A high-resolution video recording of gravitational pinch-off of the freely falling drop additionally affected with an external electrostatic field is carried out. The evolution of the shape and dynamics of motion of the structural components both the droplet itself and the satellite, as well as the secondary satellite in the absence of an electric field, is traced. Estimates of the total energy components, dominate scales and dimensionless parameters of the flow under study are given.

Keywords: drop, gravity, electrostatic field, shape evolution, high-voltage source, high-speed video filming.

DOI: 10.61011/TP.2023.11.57493.151-23

Introduction

The experimental studies of the geometry and behavior of a drop detached by gravity, that started at the close of the 19th century [1,2] and were soon supplemented by the investigation of static electric field effect [3–5], have been accelerated considerably during the past decade. The interest in electrohydrodynamic flows has been caused by several complementary factors: scientific resources of the topic, improvement of the lighting and recording test equipment, growing number of practical results in chemical, pharmaceutical and food industries, paint coatings, 3D printing and agriculture (electrospray fertilizers and crop protecting agents [6]).

The experiments recorded the pattern of neutral drop detachment from a capillary [7–9], volumetric oscillations and short capillary wave distribution over the drop surface in free falling [10,11]. Determination of growing drop shapes and calculations of the quick phase of detachment from capillary cut are described in [12,13]. Evolution of a satellite — quickly oscillating droplet, that is formed as a result of transformation of a detached neck connecting the growing drop with liquid at the capillary cut — is traced in [14]. Pattern of coalescence of a free falling drop with receiving liquid at rest without external electric and magnetic fields is visualized in [15,16].

It should be noted that general thermodynamics of heterogeneous free-surface dropping liquids has been extensively developed during past years [17,18]. At the same time, full fundamental equation system analyses methods are being improved [19] to address the internal energy transformation when free surface is destroyed [20]. The use of the singular perturbation theory to enable the compatibility condition makes it possible to calculate different-scale structural components of the evolving flows [20].

When analyzing the external electric field effect on the flow pattern during drop detachment by gravity, some typical flow conditions were highlighted [3–5]. A weak electric field effect results in shape change and volume reduction of a drop detaching from a capillary [4]. In a strong field, the flow is separated into filamentary jets and fine droplets. Analytical theory of gravitational charged drop detachment was developed in [21,22], detailed calculations of drop filling and gravitational detachment from the capillary in a weak electric field are provided in [23,24]. Investigations of the detachment pattern and size assessment of charged water drops in air, cyclohexane and transformer oil are described in [25].

In a strong electric field, single or multiple thin filaments occur on the capillary and are disintegrated into fine droplets [4,26]. High difference of potentials also causes the change in a lat surface shape of the charged liquid, where „Taylor cones“ are formed— pointed spikes, from whose tips fine droplets fly out [27].

Taking into account the scientific resources of the topic and the abundance of electrodrop technologies, of interest are detailed study of the drop detachment pattern and drop evolution tracing using a state-of-the-art flow pattern recording technique. This paper provides comparative results of high resolution visualization of flow pattern during gravitational detachment of a drop hanging on the capillary cut without and with an electric field when drop elements are kept in the flow and the flow is fully disintegrated into filamentary jets.

1. Parametrization

Previous investigations have shown that the incoming liquid first is collected into a growing pear-shaped volume on the capillary cut or solid needle (spike) tip, then a

shrinkage occurs on the surface of the volume and separates the evolving drop from the mother liquid that transforms into a neck — a thin filament (bridge, neck) connecting the growing drop with the mother liquid — residual liquid on the source [7,28–30]. When the drop is evolving and detached, the lower edge of the drop, the upper edge that contacts the neck and the center of mass also move.

In the gravitational field, the pear-shaped drop is separated from the lower edge of the neck that remains connected to the mother liquid. After neck separation, the upper convex edge of the drop is drawn inside quickly and the released drop starts falling freely at a rate U. Then the shape of the detached drop changes quickly and approaches the spherical shape whose parameters are generally used for flow parametrization.

Analysis of the full system of fluid mechanics equations, physically based equations of state and boundary-condition equations [17–20] applicable to the problems of drop detachment and falling shows that the main dimensional parameters characterizing the flow of interest include the Gibbs potentials of the drop G_d and air environment G_a (the indices show the parameter assignment), densities $\rho_{d,a}$, kinematic viscosity $\nu_{d,a}$ and dynamic viscosity $\mu_{d,a}$, full surface tension coefficient σ_d^a and surface tension coefficient

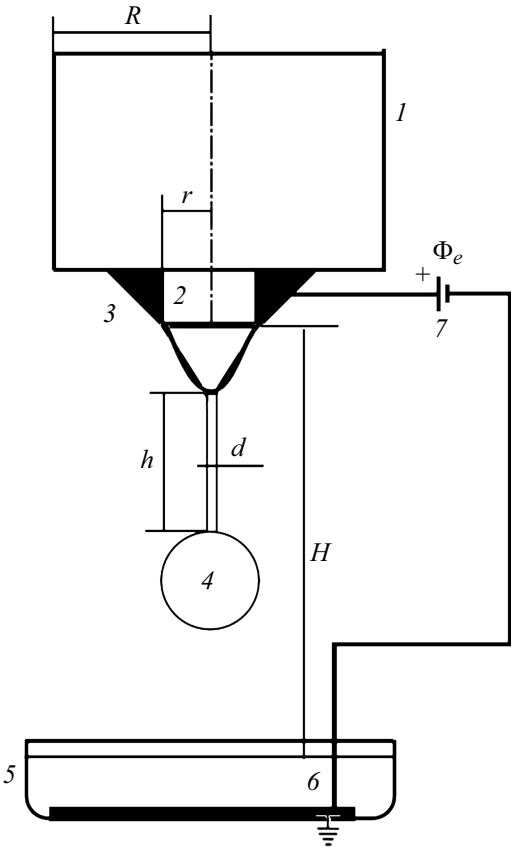

Figure 1. Experiment setup: *1* — accumulating tank, *2* — capillary, *3* — funnel-shaped electrode, *4* — drop, *5* — cell with a grounded electrode, *6* — lead wire to the grounded electrode, *7* — high voltage power supply.

normalized to the liquid density $\gamma_d^a = \sigma_d^a/\rho_d$, equivalent diameter D, surface area S_d, volume V_d, weight$M = \rho V_d$, momentum $p_d = MU$ and rate U at the time of drop detachment from the neck; available potential surface energy (APSE) $En_\sigma = \sigma S_d$, and kinetic energy $En_k = MU^2/2$. The process parameters also include the electric field energy

$$En_e = \frac{\varepsilon\varepsilon_0 V_d}{2}\left(\frac{\Phi_e}{H_e}\right)^2,$$

that depends on the drop volume V_d and applied field strength $E_e = \Phi_e/H_e$, the field is assumed as homogeneous [29,30]. Here, ε is the relative permittivity of the drop liquid, ε_0 is the universal dielectric constant, H_e is the distance between the electrodes to which voltage Φ_e is applied.

The processes that play an important role in flow restructuring include APSE En_σ transformation processes due to atomic-molecular interactions in a thin near-surface liquid layer at the interface of the liquid and individual associates of physical or chemical nature (clusters, clathrates, clustrates, strips, voids with isolated atoms, etc.) that occur spontaneously in the liquid [31]. Inhomogeneous distribution of density and other thermodynamic parameters in liquid on scales approximately equal to a molecular cluster $\delta_\sigma \sim 10^{-6}$ cm is recorded within and on the surface of liquid using high resolution instruments [32,33]. When the contacting free surfaces are destroyed during drop coalescence, APSE transforms into temperature, pressure perturbations and mechanical motion energy within the times $\tau_\sigma \sim \delta_\sigma/U$, where U is the flow rate [20]. Potential surface energy of a spherical drop En_σ is confined in a spherical layer whose thickness is $\delta_\sigma \sim 10^{-6}$ cm, volume and weight are equal to $V_\sigma = \delta_\sigma S_d$ and $M_\sigma = \rho V_\sigma$, respectively.

The basic group of length scales that are dependent on physical properties of fluids includes capillary-gravity relation $\delta_g^\gamma = \sqrt{\gamma/g}$ that is a part of dispersion equation of short surface waves [19], and a dissipative capillary scale $\delta_\gamma^\nu = \nu^2/\gamma$. A group of length scales that depend on the drop rate includes the Prandtl scale $\delta_U^\nu = \nu/U$ and capillary scale $\delta_U^\gamma = \gamma/U^2$.

Accordingly, one part of time scales in the problem includes only fluid parameters — $\tau_\gamma^\nu = \nu^3/\gamma^2$, $\tau_g^\gamma = \sqrt[4]{\gamma/g^3}$, the second part includes the drop size — $\tau_\gamma^D = \sqrt{D^3/\gamma}$, $\tau_\gamma^\nu = \nu D/\gamma$, and the third part includes the drop rate — $\tau_U^D = D/U$, $\tau_g^U = U/g$. The ratios of the basic length and time scales define the set of typical capillary dissipative rates in the problem: $U_\nu^\gamma = \delta_\gamma^\nu/\tau_\gamma^\nu = \gamma/\nu$, $U_g^\gamma = \delta_g^\gamma/\tau_g^\gamma = \sqrt[4]{\gamma g}$, $U_g^\nu = \delta_\gamma^\nu/\tau_g^\gamma = \sqrt[4]{\nu^8 g^3/\gamma^5}$, $U_\nu^g = \delta_g^\gamma/\tau_\gamma^\nu = \sqrt{\gamma^5/g\nu^6}$, and the capillary rate $U_D^\gamma = \sqrt{\gamma/D}$ [30]. Many equidimensional scales reflect a variety and complexity of processes flowing in a wide scale range — from supramolecular scales $\delta_c \sim 10^{-6}$ cm in the APSE release and accumulation processes to full flow area size.

The ratios of typical equidimensional scales define a set of traditional dimensionless process variables [15,30]. This in-

cludes the Reynolds number $\mathrm{Re} = D/\delta_U^\nu = UD/\nu$, Froude number $\mathrm{Fr} = E_k/E_p = U^2/gD$, capillary $\mathrm{Bo} = gD^2/\gamma$ and electric

$$\mathrm{Bo}_e = \frac{\varepsilon\varepsilon_0 D}{\sigma}\left(\frac{\Phi_e}{H}\right)^2.$$

Bond numbers [29,30], Ohnesorge number $\mathrm{Oh} = \nu/\sqrt{\gamma D}$, and capillary $\mathrm{We} = DU^2/\gamma$ and electric

$$\mathrm{We}_e = \frac{\varepsilon\varepsilon_0}{\rho U^2}\left(\frac{\Phi_e}{H}\right)^2.$$

Weber numbers.

The ratios of the detached drop motion rates and intrinsic rates of the problem form a set of capillary ratios $\mathrm{Ca}_1 = U/U_\gamma^\nu$, $\mathrm{Ca}_2 = U/U_g^\gamma$, $\mathrm{Ca}_3 = U/U_g^\nu$, $\mathrm{Ca}_4 = U/U_\nu^g$, $\mathrm{Ca}_5 = U/U_D^\gamma$.

The ratios of energy components form additional dimensionless combinations $\mathrm{R}_{En}^{k,\sigma} = En_k/En_\sigma$, $\mathrm{R}_{En}^{k,e} = En_k/En_e$, $\mathrm{R}_{En}^{\sigma,e} = En_\sigma/En_e$. Two first ratios are independent, and the third ratio is given for the ease of comparison of the experiment conditions.

Intrinsic scales of the problem define the requirements for selection of the dimensions of the region of interest, space-time resolution of instruments and flow pattern record time. Dimensionless ratios make it possible to evaluate the relative contribution of processes of various nature to the general flow pattern and to compare the independent experiment conditions. The large number of dimensional and dimensionless variables reflects the complexity and variety of different-scale processes that flow simultaneously.

2. Experiment procedure

The experiments have been carried out on a new bench „Simulation of Drop Flow Behavior and Structure in Electric Field“ („CDB“ — Charged Drop Behavior), as part of Unique Research Facility „Hydrophysical complex for modeling hydrodynamic processes in the environment and their impact on underwater technical objects, as well as the transport of impurities in the ocean and atmosphere (URF „HPC IPMech RAS“)“, https://ipmnet.ru/uniqequip/gfk/ [32]. During the experiments, distilled water drops were falling into a $17 \times 10 \times 7$ cm receiving plexiglass cell that was filled with water.

The diagram of the working test setup is shown in Figure 1. Liquid from plexiglass gauging tank *1* with a radius of 7 mm flows into metal capillary *2* with a diameter of $d_c = 1.0$ mm placed in funnel-shaped electrode *3*. Detaching drop *4* is formed at the capillary cut. After detachment, the free-falling drop passes the height $H_e = 50$ cm and falls into cell *5*, on the bottom of which the second electrode is placed — grounded aluminium plate *6* connected to the negative pole of power supply *7* of high voltage Φ_e.

Positive pole of power supply *7* is connected to electrode *3* contacting with metal capillary *2*. The formed drop detaches by gravity or under the combined effect of gravitational and electric fields. The proprietary high voltage power supply allows to change the applied voltage within $0 < \Phi_e < 30$ kV with increment 2 kV. These experiments were carried out at $\Phi_e = 15$ kV or with switched off power supply. The voltage setting error is 1 kV.

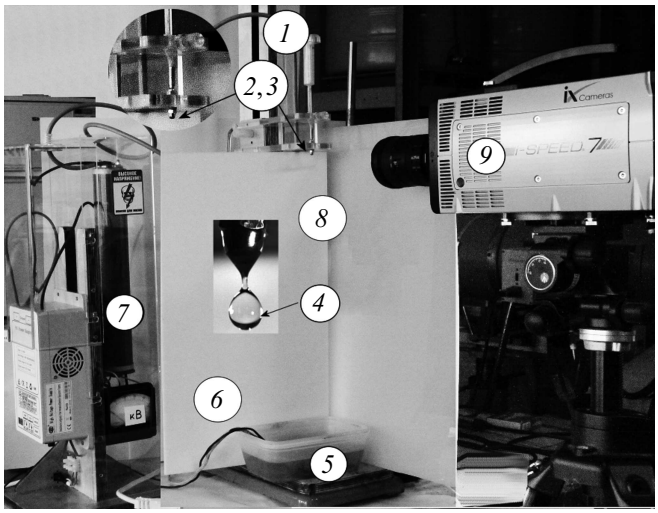

Figure 2. Experimental bench: *1* — tank, *2, 3* — capillary in the funnel-shaped electrode, *4* — drop, *5* — water-filled cell, *6* — lead wires to the grounded electrode, *7* — high voltage power supply, *8* — compound screen, *9* — video camera.

The setup photo is shown in Figure 2. Here, *1* is the accumulating tank that maintains the constant liquid flow rate in capillary *2*. The scaled up fragment of the setup containing the capillary built in funnel-shaped electrode *3* is shown in the detail. Drop *4* detached from the capillary cut falls into receiving cell *5*. Electrode *6* on the cell bottom is connected to the negative pole of constant high voltage power supply *7*. To illuminate the flow pattern, Optronis MultiLED 7700 lm matrix fixtures were placed behind matte screens *8* („diffusion distributed counter and side light“ method).

The flow pattern was recorded by video camera *9* (*i*-speed 717) installed on a tripod head with four degrees of freedom. Frame rate for the experiments was equal to 20 000 frames per second. The video recording mode provided a linear resolution of at least 0.01 mm. Linear dimension measurement error on video frames was equal to 0.05 mm, that was approximately the half of the outline thickness the item to be measured (drop, neck). The camera was started at the point of time when the mother liquid flow rate was maximum before the drop detachment (after occurrence of the clearly pronounced neck meaning that the active drop separation phase has started). The video records were stored in the computer memory for future reference. For data processing, the laboratory system of coordinates x, z was used,where the z axis is directed downwards, and its origin coincides with the upper edge of the video frame.

Table 1. Dimensionless variables of the problem

Φ_e, kV	Re	Fr	Bo	Bo_e	Oh	We	We_e	$R_{En}^{k,\sigma}$	$R_{En}^{k,e}$	$R_{En}^{\sigma,e}$
0	1972	1.8	66 220	0	0.0015	9.0	0	0.75	∞	∞
15	2170	13.5	20 030	0.03	0.002	19.7	0.0015	1.64	340	207

Table 2. Capillary ratios of typical rates

Φ, kV	Ca_1	Ca_2	Ca_3	Ca_4	Ca_5
0	1972	2.0	$4 \cdot 10^5$	0.01	3.0
15	2170	4.0	$8.0 \cdot 10^5$	0.01	4.4

In this set of experiments, distilled water was continuously flowing into the capillary at constant flow rate $Q = 0.0054$ ml/s, while the capillary outlet flow rate (diameter $d_c = 1$ mm) was$u = 6.8$ mm/s. For these experiments, the free fall height of the drops was equal to $H = 50$ cm.

In the experiments without electric field, the incoming liquid is kept at the capillary cut for some time during the drop formation. Then a shrinkage occurs on its surface that separates the mother liquid. A slowly lowering drop-shaped volume and a waist — a gradually extended and non-uniformly thinned filament — are formed under the neck. The bottom of the neck that is adjacent to the drop is getting thinned much faster and finally is separated. At the time of detachment from the neck, the drop rate is $U = 0.33$ m/s.

The neck residue starts pulling together forming a set of spherical swells. The mother liquid surface is rising quickly resulting in thinning and separation of the top of the neck.

Then the drop and neck residue evolve independently. The detached pear-shaped liquid volume is pulling together quickly and oscillates. During the restructuring process, the drop takes a shape of a $D = 6.0$ mm sphere for a short time.

The drop detachment pattern in the electrostatic field ($\Phi_e = 15$ kV) differs drastically. Here, a club-shaped „drop−neck“ assembly first gets detached from the mother liquid. Then, the bottom of the neck gets thinned and separated from the drop. When the drop gets detached from the lower end of the neck, its rate is $U = 0.66$ m/s. The drop shape changes quickly and its diameter in the spherical phase is equal to $D = 3.9$ mm.

The values of the main dimensionless variables describing the experiment conditions are listed in Table 1.

Capillary numbers — ratios of drop rate to the typical rates of the problem — are listed in Table 2.

The features introduced by the electric field include considerable difference in the values of traditional dimensionless variables characterizing the flow behavior and geometry. The difference reflects the drop size reduction and drop rate increase at the time of detachment from the neck. The detachment process behavior is traced further in description of the experiments.

3. Gravitational drop detachment

Gravitational drop detachment (without electric field) processes are illustrated by the video samples in Figure 3. Immediately before the detachment, the mother liquid takes a tapered shape, to a tip of which a cigar-shaped neck is adjacent. The neck has a thinned end that contacts the convex drop surface.

The slowly growing drop (the lower edge motion rate is $U = 15$ cm/s) gets detached from the lower thin end of the tapered neck that connects the drop to the mother liquid, and then accelerates quickly ($U = 0.33$ m/s, Figure 3, *a*). 0.5 ms after the detachment, the upper edge of the drop gets flattened (Figure 3, *b*), the neck becomes shorter with its lower sharp end folding into a spherical droplet (transverse diameter is $d_1^s = 0.7$ mm) separated by a waist from the second droplet that starts growing (transverse diameter is $d_2^s = 0.6$ mm). The mother liquid moves up by $\Delta h_m = 0.2$ mm. After another 0.5 ms (Figure 3, *c*), the neck becomes shorter and its top is thinned.

The mother liquid keeps mowing upwards and covers the distance of $\Delta h_m = 0.6$ mm. The tapered outline of the mother liquid transforms to the parabolic outline (Figure 3, *c*). 1.2 ms after the drop detachment from the lower neck end, the mother liquid that is getting pulled together separates from the thinned upper end of the neck. The moving upper edge of the falling drop takes a convex shape.

The time variability of the neck height and thickness in the midsection is demonstrated by the curves in Figure 3, *e*. After the drop detachment to $t = 1.8$ ms, neck height h decreases gradually, and thickness d grows slowly remaining near 0.4 mm. Then the height reduction and thickness growing rates increase considerably, their dimensions get closer and coincide at $t = 4$ m, then the next cycle starts from height growth and thickness reduction.

Video samples illustrating further evolution of the detached neck and free drop are shown in Figure 4. Fully detached neck transforms into a coalesced fine droplet chain (Figure 4, *a*). After detachment, a drop with height $h_d = 5.8$ mm and diameter $D = 6.1$ mm still has a vertically elongated axially symmetric shape with a flat top and convex base. A neck, that is pulled together, with $h_s = 2.7$ mm and$d_s = 0.8$ mm forms a satellite composed of four droplets with diameters of $d_{1-4}^s = 0.4, 0.6, 0.7, 0.8$ mm (Figure 4, *a*, $t = 2$ ms).

Within the interval between adjacent frames $\Delta t = 5.3$ ms, the shape of detached elements changes dramatically: the drop is pulled together vertically ($h_d = 4.9$ mm, transverse diameter$d = 5.3$ mm), and the satellite includes a spherical portion ($d_s = 0.8$ mm) and two thin cylinders adjacent to the lower and upper poles with $h_s^c = 1.1$ mm (Figure 4, *b*). A droplet appears in the center of the lower cylinder and is quickly drawn in. Then, a finer secondary satellite is released upwards from the upper cylinder and quickly approaches the mother liquid surface and jumps back to the satellite that takes an

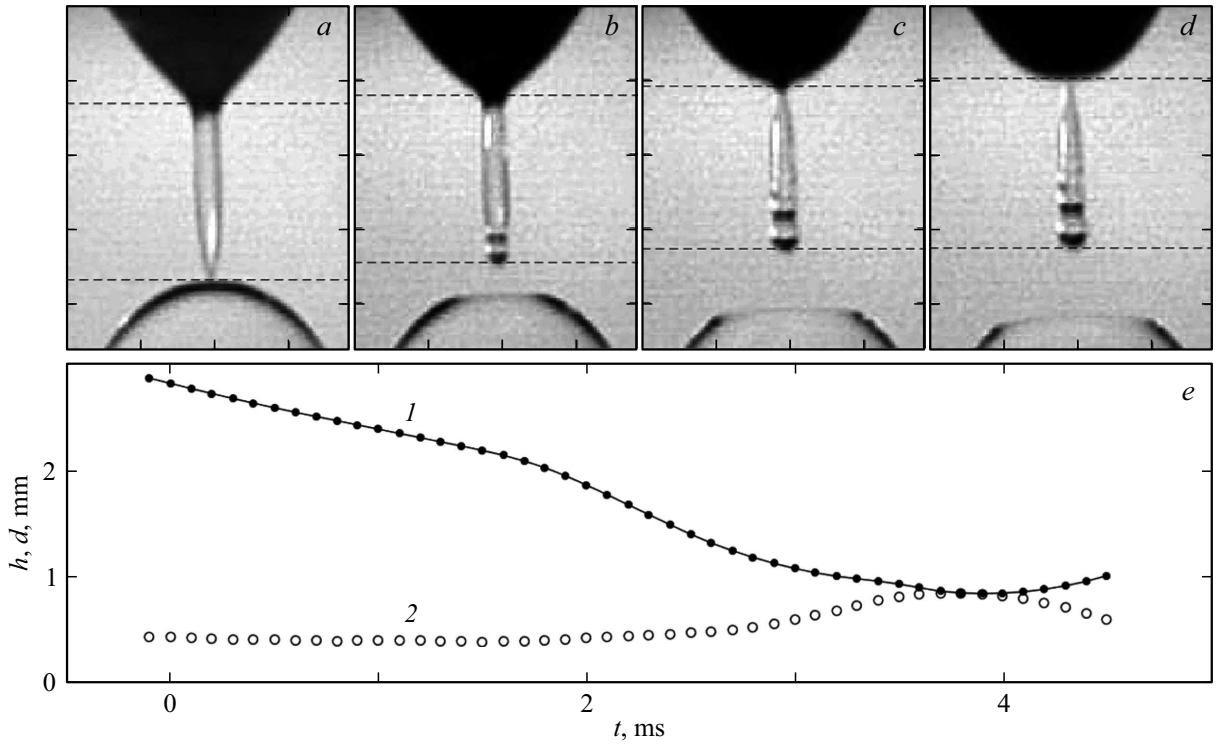

Figure 3. Uncharged drop detachment pattern: *a*–*d* — $t = 0$, 0.5, 1.0 and 1.2 ms from the time of detachment of the lower neck end; *e* — height h (curve *1*) and transverse diameter d (curve *2*) in the neck midsection at 4.5 ms. Sampling interval — 100 μs.

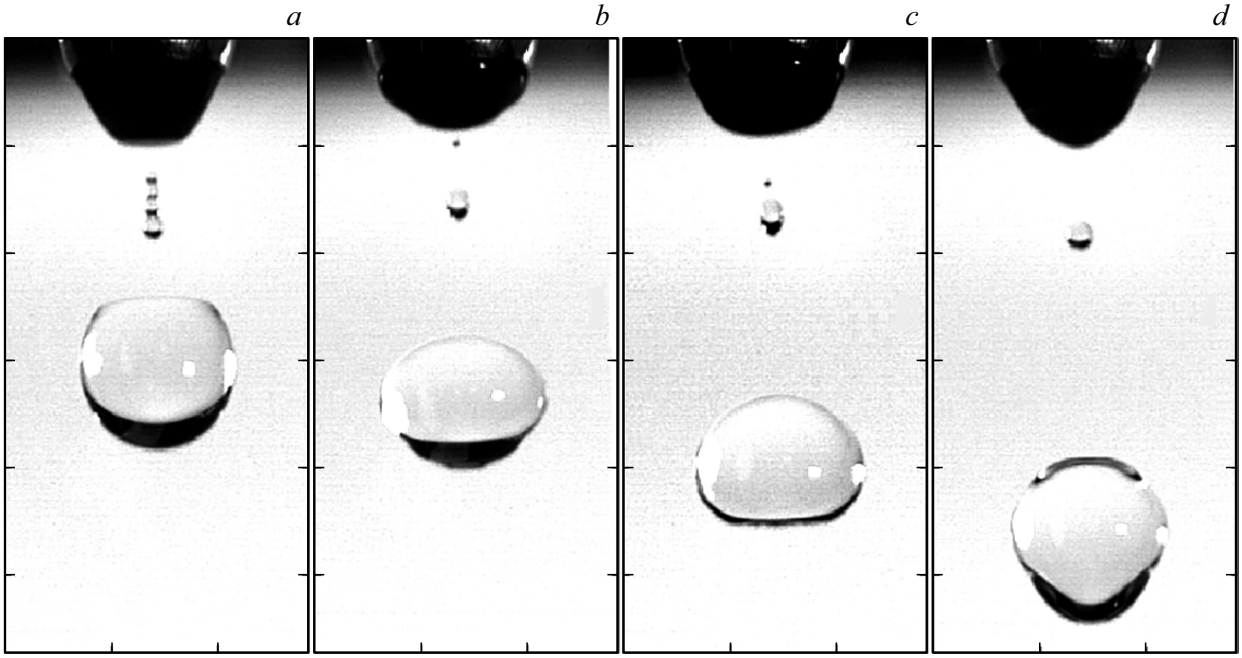

Figure 4. Uncharged drop and satellite motion pattern: *a*–*d* — $t = 2.0$, 7.3, 12.8, 19.5 ms, the time is counted from the time of drop separation from the lower neck end, scale division 4 mm.

increasingly complex shape due to partial coalescence of cylindrical sections with the central spherical section (Figure 4, *c*). The mother liquid shape is also changing contiguously.

The shape of the main drop also changes considerably, its top becomes convex and the bottom becomes flat (Figure 4, *c*, $t = 12.8$ ms, $h_d = 4.9$ mm, $d = 6.5$ mm). After a slight rise, the primary satellite with $h_s = 1.5$ mm and

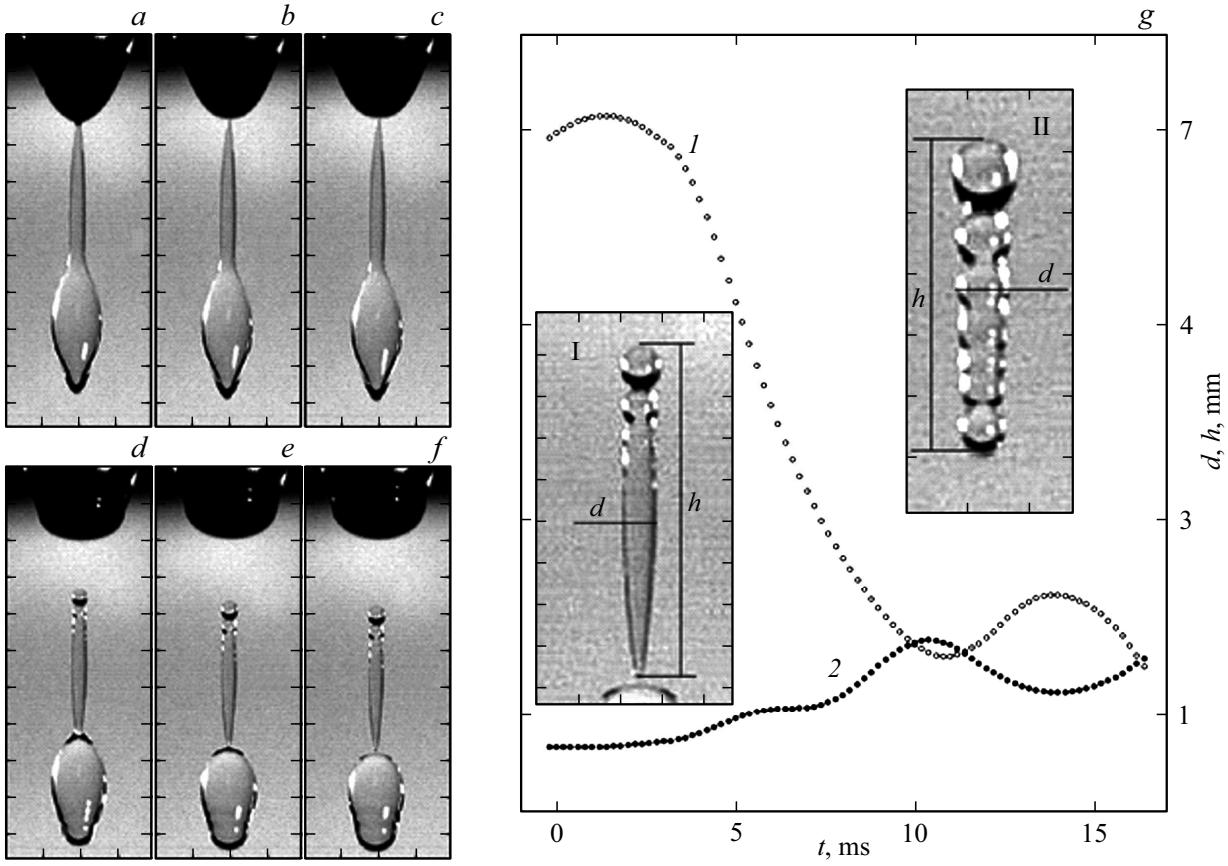

Figure 5. Charged drop detachment pattern in the electrostatic field ($\Phi = 15$ kV): *a–f* — $t = -0.7$, -0.2, 0, 2.3, 3.0, 3.3 ms (from the time of detachment of the upper satellite edge), division is 2 mm. *g* — height h (curve *1*) and transverse diameter d (curve *2*) of the neck in the vertical midsection. Data sampling interval is — 200 μs. Details: scaled up neck after complete detachment at $t = 3.3$ (I) and 5.2 (II) ms. Division is 1 mm.

$d_s = 0.9$ mm starts moving downwards in a regular manner. At $t = 19.5$ ms, the primary and secondary satellites merge together and form a single convex droplet with $h_s = 1.1$ mm and $d_s = 0.9$ mm. The primary drop extends vertically and the symmetry relative to the horizontal plane is lost.

During falling (during the first $t = 17.5$ ms), the satellite positions relative to the upper edge of the pattern are $h_s^u = 7.1$, 6.6, 7.2 7.8 mm at $t = 2.0$, 7.3, 12.8, 19.5 ms, respectively. Positions of the lower drop edge are equal to $h_d^l = 15.3$, 16.1, 17.4 and 21.4 mm. Therefore, the average rates of the drop and satellite at $\Delta t = 17.5$ ms are equal to $\overline{U} = 35$ and $\overline{u}_s = 5$ cm/s. Qualitatively, the flow pattern corresponds to the pattern observed in [3,9].

The observed difference in the drop and satellite rates may be caused by the electrostatic interaction between the satellite and spontaneously charged drop and liquid in the capillary (it is generally assumed that free water surface is negatively charged [33,34]). However, the charge sign may change inflows or under the effect of internal flows that are formed when APSE transforms into other types with change of the satellite shape [20], that requires more detailed study.

4. Charged drop detachment

The flow pattern during the drop detachment in the electric field illustrated by the video records in Figure 5 differs considerably. The shape of the liquid accumulated at the capillary cut becomes club-shaped with sharp ends (Figure 5, *a, b*), instead of the pear-like shape without field. Flow elements become more elongated than those for the gravitational detachment (Figure 3).

In the electric field, the neck separation sequence changes: here, the whole neck together with the sharpened swell, from which the detaching drop is formed, is first separated from the mother liquid (Figure 5, *c*). Before the detachment, the contact area between the neck and mother liquid is thinned. Parts of the detached liquid volume behave differently. The upper narrow end of the neck is rounded, while the lower end is thinned (Figure 5, *d*). The lower volume is rounded and forms a pear-shaped drop, while the upper volume is pulled together and forms a series of growing spherical swells (Figure 5, *d, e*).

The lower and upper ends of the growing drop continue keep getting rounded. Short capillary waves run over the drop surface and are clearly pronounced near the contact

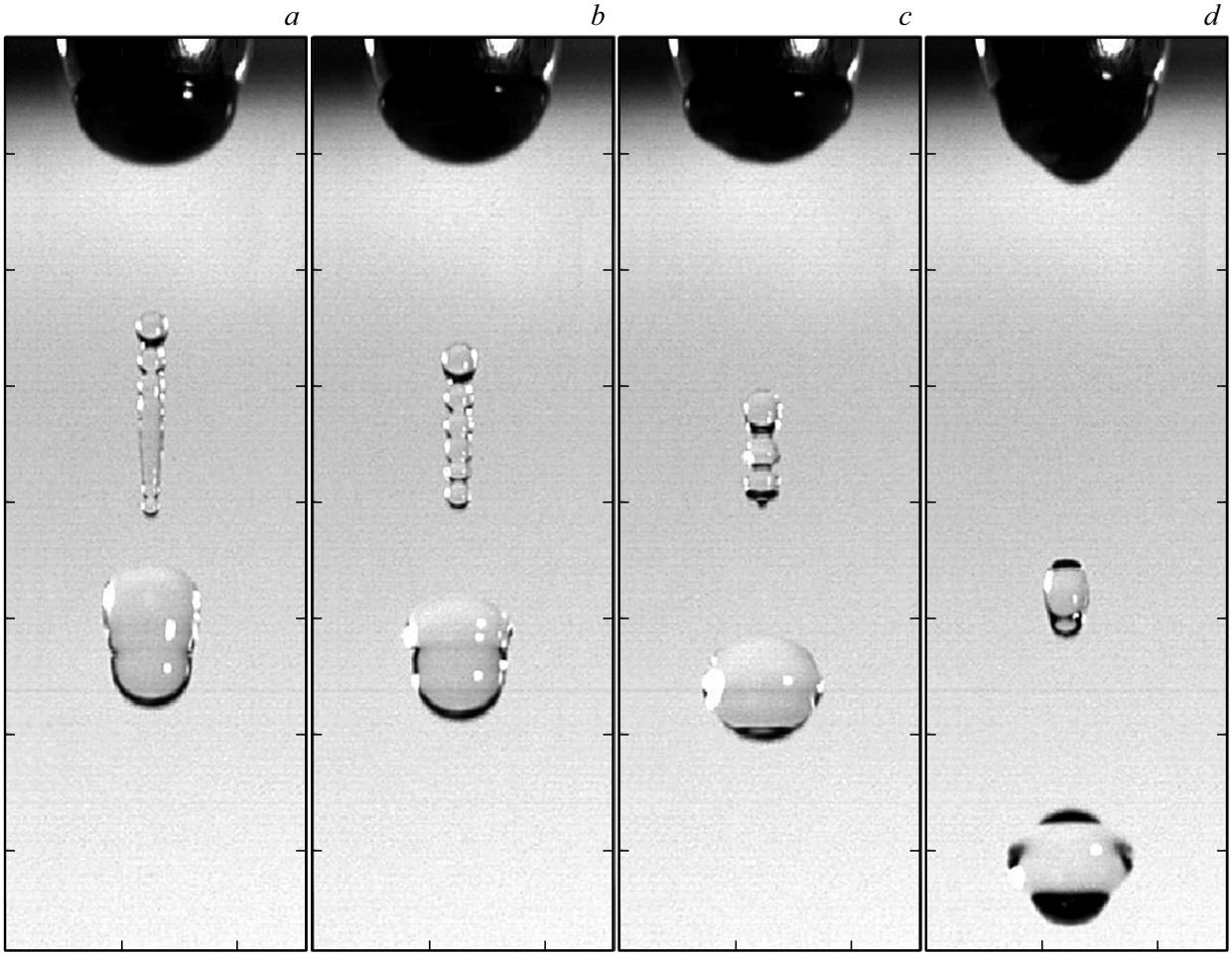

Figure 6. Charged drop and satellite movement in the electrostatic field ($\Phi_e = 15$ kV): *a*–*d* — $t = 4.5$, 5.6, 7.2, 14.8 ms, the time is counted from the detachment of the upper neck end from the mother liquid.

with the neck and in the drop bottom (Figure 5, *d*–*f*). Drop detachment from the neck occurs at $t = 3.3$ ms. After the detachment, the neck is slightly elongated up to $t = 1.4$ ms, then gradual reduction occurs up to $t = 10.8$ ms, then smooth rise and drop with a peak at $t = 14$ ms occur (Figure 5, *g*, curve *1*).

In the midsection, the neck grows non-monotonically beginning from the detachment (curve *2*, Figure 5, *g*) to about $t = 10.8$ ms, where h is as low as possible. Then a drop occurs to the lowest point at $t = 14$ ms corresponding with the maximum h time. At $t = 10$, 11.4, 16.4 ms, the horizontal dimension coincides with the vertical dimension — the neck takes a spherical shape. Throughout the observation time, the neck evolution moves towards compression into a compact volume successively taking the shapes of elongated and compressed bodies, including multi-link shapes (Figure 5, *g*, Detail II, Figure 6).

During its evolution, the drop is also gradually compressed and becomes compact: Figure 6 shows a time interval, during which the vertical dimension of the drop is reduced from 4.8 (Figure 6, *a*) to 3.8 mm (Figure 6, *d*); and capillary waves are running on the drop surface in this case (Figure 6, *a*–*c*). The neck outline that keeps its tapered shape is filled with spherical swells (Figure 6, *a*, the upper swell diameter is $d_u^s = 1.2$, the lower swell diameter is $d_l^s = 0.7$ mm) and waists with an interval decreased from top to bottom.

The neck residue outline with $h_s = 5.9$ and maximum $d_s = 1.6$ mm ($t = 5.6$ ms, Figure 6, *b*) contains six swells. The primary drop height decreases to $h_d = 4.4$ mm, and the transverse dimension increases to $d = 3.8$ mm. Only three spherical swells with $d_{1,2,3}^s = 1.4$, 1.3, 1.4 mm are kept in the neck residue with the total height of 1 $h_s = 4.1$ mm. A small ball with a diameter of $d_l^s = 0.3$ mm occurs on the lower end of the neck residue (Figure 6, *c*). The drop shape approaches the spherical shape with the height and width, respectively, equal to $h_s = 3.8$ and 4.2 mm. The drop outline contains swells near the equator.

At the end of the observation interval, the neck residue pulls together into a body of rotation (height and thickness are $h_s = 2.7$ and $d_s = 1.6$ mm, respectively) with waists separating the upper section ($h_s^u = 0.3$ mm) and lower section ($h_s^l = 0.8$ mm) from the convex central body ($t = 14.8$ ms, Figure 6, *e*). The primary drop (height

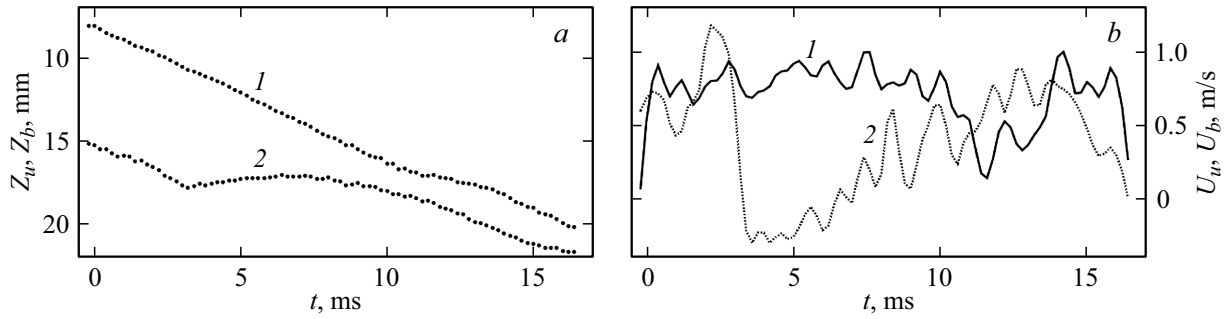

Figure 7. Position (a) and rate (b) of the upper (1) and lower (2) neck ends when the charged drop gets detached. Time — from the detachment of the lower neck end.

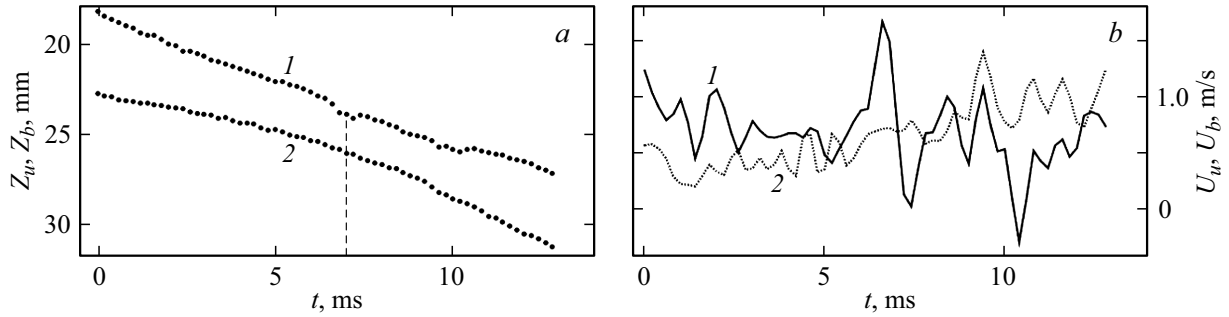

Figure 8. Change of position (a) and rate (b) of the upper (1) and lower (2) edges of the charged drop. Time — from the detachment of the lower neck end.

4.0 mm, transverse diameter 4.2 mm, Figure 6, d) loses its symmetry about the horizontal plane at the maximum transverse diameter level (height of the upper section $h_d^u = 1.7$ mm of the lower section — $h_d^l = 2.3$ mm. Swells at the maximum diameter level in the right and let parts of the drop (Figure 6, d) are different in size.

Rates of fall of the primary drop and neck residue differ significantly — the distance between their centers of mass in Figure 6 are equal to $\Delta z_m = 7.2$, 7.4, 8.1, 9.4 mm, respectively, corresponding to the rates of divergence $u_z^m = 0.2$, 0.4 and 0.2 m/s. Distances between the lower neck ends and tip of the primary drop are$\Delta z_d = 1.7$, 2.9, 4.5, 5.9 mm; therefore, the rate of divergence is equal to $u_d^m = 1.1$, 1.0 and 0.2 m/s. Comparison of values shows that the change of shapes and dimensions of the separated elements has a considerable effect on the flow geometry.

Geometry of motion of the flow components after separation (Figure 6) shows that the upper neck end moves steadily enough, its coordinate over time is approximated by $Z_u = 0.7t + 8.5$ (Figure 7, a, curve *1*). Within 0–10 ms, the instantaneous rate fluctuates near the average 0.7 m/s (Figure 7, curve *1*).

At the same time, the lower neck end moves non-uniformly under the surface tension and gravity. The distance of the lower end of the compressing neck from the upper frame edge is approximated by two time dependences — (Figure 7, a, curve *2*) linear $Z_b = 0.75t + 15.3$ ($t \le 3.2$ ms) and quadratic $Z_b = 0.04t^2 + 0.52t + 18.6$ ($t > 3.2$ ms). The instantaneous motion rate curve (Figure 7, b, curve *2*) suggests that fast and slow fluctuations of the lower end position are alternated reflecting complex behavior of thin processes in the neck residue. Within 4.5–10.5 ms, rate oscillations of both ends can be seen whose peaks and valleys coincide in time (Figure 7, b, curves *1* and *2*). In the rate fluctuation spectra of this interval, a fundamental frequency 750 Hz is present.

Behavior of the charged drop is illustrated by the drop edge position curves (Figure 8) after detachment from the movement of the upper and lower edges is approximated by weakly non-linear polynomials, respectively, $-0.013t^2 + 0.86t + 18.26$ (Figure 8, a, curve *1*) and $0.04t^2 + 0.18t + 23.0$ (Figure 8, a, curve *2*). Due to the difference in the acceleration signs (quadratic terms), the edges first get closer up to $t_c = 7.0$ ms (vertical dashed line in Figure 8, a), and then diverge.

The rates of lowering of the lower and upper drop edges within this time range differ considerably in value and pattern of oscillations (Figure 8, b). Both edges generally move down, though, very non-uniformly, but the upper edge on individual time intervals (near 7.0 and 10.0 ms) is inverted. Both curves within 8–13 ms contain almost synchronous rate fluctuations at the fundamental frequency of 600 Hz (according to the spectral analysis).

5. Discussion of findings

The analysis of findings shows that in these experimental conditions when the drop was formed at the capillary cut with a diameter of $d = 1.0$ mm at continuous liquid inflow with a low rate of $Q = 0.0054$ ml/s and mass flow rate$u = 6.8$ mm/s, the time of charged and uncharged drop occurrence was the same and equal tot$_f = 90$ ms.

For the gravitational detachment, the free drop diameter (in the spherical phase) was equal to $D = 6.0$ mm, area and volume — $S_d = 1.1$ cm^2 and $V_d = 114.2$ mm^3, weight$M = 0.11$ g, rate after detachment from the neck — $U = 0.33$ m/s, kinetic and surface energies are equal to $En_k^d = 6.1 \cdot 10^{-6}$ and $En_\sigma^d = 8.2 \cdot 10^{-6}$ J, respectively. Diameter and volume of the satellite into which the free neck folded were equal to $d_s = 1.2$ mm, $V_s = 0.9$ mm^3. The key elements of the drop detachment pattern — neck — according to the author's terminology, satellites that occur during detachment of the aqueous potassium permanganate solution or aqueous potassium bichromate solution drop whose photos were first taken by Rayleigh in 1890 [35], in future were repeatedly recorded in increasingly more detail with improvement of instruments. Patterns of the funnel-shaped neck transformation into a „string of spherical beads" during water drops detachment are shown in [7], satellite shape evolution and secondary satellite behavior — are shown in [36]. Flow patterns for detachment of water and alcohol drops are compared in [37], for detachment of water drops and various oil drops — are compared in [9]. General properties of the observed flow pattern — neck formation, drop detachment from its lower edge, neck detachment from the liquid residue at the capillary, transformation of a smooth funnel-shaped neck into a ridged shape and then into a single droplet — agree with the data of [7,9,35–37], however, the number of elements, transformation behavior and movements may differ significantly. The nature of flow parameter variability depending on the test setup and conditions needs closer examination.

Diameter of the drop detached in the electric field ($\Phi_e = 15$ kV) was $D = 3.75$ mm, surface areas was $S_d = 0.34$ cm^2, volume was $V_d = 27.6$ mm^3, and weight was $M = 0.02$ g. The rate of charged drop after the detachment was equal to $U = 0.66$ m/s.

Kinetic, surface and electric energies of the drop were equal to $En_k^d = 4.1 \cdot 10^{-6}$, $En_\sigma^d = 2.3 \cdot 10^{-6}$ and $En_e^d = 1.2 \cdot 10^{-8}$ J, respectively. The detached neck transforms into the satellite — a ball with a diameter of $d_s = 1.8$ mm, surface area and volume of $V_s = 3.0$ mm^3, that falls at a rate of $U_s - 0.86$ m/s. Kinetic, surface and electric energies of the satellite are equal to $En_k^s = 1.1 \cdot 10^{-6}$, $En_\sigma^s = 7.4 \cdot 10^{-7}$ and $En_e^s = 2.0 \cdot 10^{-9}$ J, respectively.

The experiments show that the external electric field has a significant impact on detachment, shapes of the flow components (drops and satellites) that are detached and formed over time, ratio of drop energy components. In the gravitational field, the drop detaches from the lower neck end. In the external electrostatic field with a voltage of $\Phi_e = 15$ kV, the upper neck edge first detaches from the mother liquid, and then the neck−drop system is disintegrated into independently moving components with a delay of several milliseconds. In this case, a small protrusion that is formed on the lower edge of the detached neck does not transform into a secondary satellite. Here, the variability of flow parameters is expressed even more clearly than for merely gravitational detachment.

The obtained data may be used as a basis for further study of the drop and satellite behavior in flight, control of drop formation, dimensions and rate, measurement of the electric field effect on drop coalescence with the receiving liquid, detailed description of the momentum, energy and substance transport mechanisms.

Conclusion

A unit has been made to carry out high resolution visualization of quickly evolving flow pattern during detachment from the capillary, drop formation and disintegration in the gravitational and external electrostatic field with applied voltage within $0 < \Phi_e < 30$ kV.

The effect of $\Phi_e = 15$ kV electric field on the flow structure, component shapes and motion behavior of detached millimeter drops and accompanying satellites was traced for the first time.

Values of various energy components were evaluated for the drop and satellites formed during detachment in the gravitational field and electrostatic field acting simultaneously.

Funding

The study was supported financially by the Russian Science Foundation (project 19-19-00598-P „Hydrodynamics and Energy of Drop and Drop Jets: Formation, Motion, Disintegration and Interaction with the Contact Surface", https://rscf.ru/project/19-19-00598/).

Acknowledgments

The experiments were carried out using the „CDB" bench included in the Unique Research Facility „Hydrophysical complex for modeling hydrodynamic processes in the environment and their impact on underwater technical objects, as well as the transport of impurities in the ocean and atmosphere (URF „HPC IPMech RAS")".

The authors would like to thank Doctor of Physics and Mathematics N.G. Solovieva for the assistance in the development of the experiment procedure and valuable advice.

Conflict of interest

The authors declare that they have no conflict of interest.

References

[1] F. Guthrie. Proc. R. Soc. Lond., **13**, 457 (1864). DOI: 10.1098/rspl.1863.0091
[2] J.J. Thomson, H.F. Newall. Proc. R. Soc. Lond., **29**, 417 (1885). DOI: 10.1098/rspl.1885.0034
[3] J. Zeleny. Phys. Rev., **3** (2), 69 (1914). DOI: 10.1103/physrev.3.69
[4] J. Zeleny. Proc. Cambridge Philos. Soc., **18** (1), 71 (1915).
[5] J. Zeleny. Phys. Rev., 10 (1), 1 (1917). DOI: 10.1103/physrev.10.1
[6] S.E. Law. IEEE Transactions on Industry Applications, **IA-19** (2), 160 (1983). DOI: 10.1109/tia.1983.4504176
[7] D. Peregrine, G. Shoker, A. Symon. J. Fluid Mech., **212** (1), 25 (1990). DOI: 10.1017/S0022112090001835
[8] X. Zhang, O.A. Basaran. Phys. Fluids, **7** (6), 1184 (1995). DOI: 10.1063/1.868577
[9] Yu.D. Chashechkin, V.E. Prokhorov. J. Appl. Mech. Tech. Phys., **57** (3), 402 (2016). DOI: 10.1134/S0021894416030032
[10] A.I. Korshunov. Fluid Dyn., **50** (4), 585 (2015). DOI: 10.1134/S0015462815040134
[11] A.V. Kistovich, Yu.D. Chashechkin. Atm. Oceanica Phys., **54** (2), 182 (2018). DOI: 10.7868/S0003351518020095
[12] J. Eggers. Rev. Modern Phys., **69** (3), 865 (1997). DOI: 10.1103/revmodphys.69.865
[13] E. Wilkes, S.D. Phillips, O.A. Basaran. Phys. Fluids, **11** (12), 3577 (1999). DOI: 10.1063/1.870224
[14] F. Bierbrauer, N. Kapur, M.C.T. Wilson. ESAIM: Proceed., **40**, 16 (2013). DOI: 10.1051/proc/201340002
[15] Yu.D. Chashechkin, A.Y. Ilinykh. Axioms, **12** (4), 374 (2023). DOI: 10.3390/axioms12040374
[16] P.K. Notz, A.U. Chen, O.A. Basaran. Phys. Fluids, **13** (3), 549 (2001). DOI: 10.1063/1.1343906
[17] R. Feistel. Ocean Sci., **14**, 471 (2018). DOI: 10.5194/os-14-471-2018
[18] A.H. Harvey, J. Hrubý, K. Meier. J. Phys. Chem. Refer. Data, **52**, 011501 (2023).
[19] L.D. Landau, E.M. Lifshits. *Teoreticheskaya fizika. Tom VI. Gidrodinamika* (Nauka, M., 1986) (in Russian)
[20] Y.D. Chashechkin. Axioms, **10** (4), 286 (2021). DOI: 10.3390/axioms10040286
[21] A.A. Zemskov, S.O. Shiryaeva, A.I. Grigor'ev. J. Colloid Interface Sci., **158** (1), 54 (1993). DOI: 10.1006/jcis.1993.1228
[22] A.I. Grigor'ev, S.O. Shiryaeva. J. Aerosol Sci., **25** (6), 1079 (1994). DOI: 10.1016/0021- 8502(94)90203-8
[23] P.K. Notz, O.A. Basaran. J. Colloid Interface Sci., **213** (1), 218 (1999). DOI: 10.1006/jcis.1999.6136
[24] R.N. Savage, G.M. Hieftje. Rev. Sci. Instrum., **49** (10), 1418 (1978). DOI: 10.1063/1.1135281
[25] T. Takamatsu, M. Yamaguchi, T. Katayama. J. Chem. Engin. Jpn., **16** (4), 267 (1983). DOI: 10.1252/jcej.16.267
[26] M. Cloupeau, B. Prunet-Foch. J. Aerosol Sci., **25** (6), 1021 (1994). DOI: 10.1016/0021-8502(94)90199-6
[27] J. Rosell-Llompart, J. Grifoll, I.G. Loscertales. J. Aerosol Sci., **125**, 2 (2018). DOI: 10.1016/j.jaerosci.2018.04.008
[28] X. Zhang, O. Basaran. J. Fluid Mech., **326**, 239 (1996). DOI: 10.1017/S0022112096008300
[29] R.T. Collins, J.J. Jones, M.T. Harris, O.A. Basaran. Nature Phys., **4** (2), 149 (2008). DOI: 10.1038/nphys807
[30] P.K. Notz, A.U. Chen, O.A. Basaran. Phys. Fluids, **13** (3), 549 (2001). DOI: 10.1063/1.1343906
[31] C.R. Anthony, H. Wee, V. Garg, S.S. Thete, P.M. Kamat, B.W. Wagoner, E.D. Wilkes, P.K. Notz, A.U. Chen, R. Suryo, K. Sambath, J.C. Panditaratne, Y.-C. Liao, O.A. Basaran. Annu. Rev. Fluid Mech., **55**, 707 (2023). DOI: 10.1146/annurev-fluid-120720-014714
[32] Unique Research Facility „Hydrophysical complex for modeling hydrodynamic processes in the environment and their impact on underwater technical objects, as well as the transport of impurities in the ocean and atmosphere (URF „HPC IPMech RAS")" site http://www.ipmnet.ru/uniqequip/gfk/#equip.
[33] P. Lenard. Anal. Phys., **370**, 629 (1921). DOI: 10.1002/andp.19153521203
[34] S.I. Karakashev, N.A. Grozev. Coatings, **10**, 1003 (2020). DOI: 10.3390/coatings10101003
[35] Lord Rayleigh. Nature, **44** (1133), 249 (1891). DOI: 10.1038/044249e0
[36] Yu.D. Tchashechkin, V.E. Prokhorov. Doklady RAN.**454** (1), 31 (2014).(in Russian) DOI: 10.1134/S1028335814010017
[37] V.E. Prokhorov,Yu.D. Tchashechkin. Izvestiya RAN. MZhG, **4**, 109 (2014). (in Russian)

Translated by Ego Translating